Journal of
Mechanics of
Materials and Structures

IMPROVED HYBRID ELEMENTS FOR STRUCTURAL ANALYSIS

C. S. Jog

Volume 5, No. 3 March 2010

mathematical sciences publishers

JOURNAL OF MECHANICS OF MATERIALS AND STRUCTURES
Vol. 5, No. 3, 2010

IMPROVED HYBRID ELEMENTS FOR STRUCTURAL ANALYSIS

C. S. JOG

Hybrid elements, which are based on a two-field variational formulation with the displacements and stresses interpolated separately, are known to deliver very high accuracy, and to alleviate to a large extent problems of locking that plague standard displacement-based formulations. The choice of the stress interpolation functions is of course critical in ensuring the high accuracy and robustness of the method. Generally, an attempt is made to keep the stress interpolation to the minimum number of terms that will ensure that the stiffness matrix has no spurious zero-energy modes, since it is known that the stiffness increases with the increase in the number of terms. Although using such a strategy of keeping the number of interpolation terms to a minimum works very well in static problems, it results either in instabilities or fails to converge in transient problems. This is because choosing the stress interpolation functions *merely* on the basis of removing spurious energy modes can violate some basic principles that interpolation functions should obey. In this work, we address the issue of choosing the interpolation functions based on such basic principles of interpolation theory and mechanics. Although this procedure results in the use of more number of terms than the minimum (and hence in slightly increased stiffness) in many elements, we show that the performance continues to be far superior to displacement-based formulations, and, more importantly, that it also results in considerably increased robustness.

1. Introduction

Ever since the pioneering work of Pian et al. [1984; 1986], it is known that hybrid stress-based formulations, which are based on a two-field variational formulation involving displacement and stresses, are much less susceptible to locking than standard displacement-based formulations. In fact, Simo et al. [Simo et al. 1989, p. 70], while discussing their interpolation procedure for membrane stresses state, "...the interpolation procedure is closely related to the mixed formulation for plane stress proposed by Pian and Sumihara (which appears to be optimal)." As discussed in [Jog and Kelkar 2006], conventional shell elements suffer from a number of shortcomings such as the need to develop reduced constitutive models, the need for transition elements while interfacing with brick elements, significant reformulation for thick shells etc. Thus, recently, there has been a significant effort towards the development of three-dimensional solid-shell elements with only displacement degrees of freedom. However, since a kinematic assumption is being made in their development, even these elements would need a significant reformulation for thick shells.

Since no kinematic assumption is being made in the development of hybrid elements, since the treatment is full three-dimensional with no plane-stress or any other such assumption being made (which allows for easy implementation of material nonlinearities), since there are no stabilization parameters that need to be adjusted as in some "strain-based" formulations, and since they are relatively much

Keywords: hybrid finite elements, linear/nonlinear, static/transient, structural analysis.

more immune to locking, and converge more rapidly than standard displacement-based elements, hybrid elements can be used very effectively (with no modification of the formulation) to model problems as diverse as beams/plates/shells on one hand, and problems involving "chunky" geometries on the other. Even from a user viewpoint, since the stress degrees of freedom are condensed out at an element level, the formulation ultimately involves only displacement degrees of freedom, so that the same input data (nodal coordinates, connectivity, boundary conditions etc.) that is used for conventional displacement-based elements can be used for the hybrid formulation also. The drawback of hybrid elements that is often mentioned is the need to invert a small matrix to construct the element stiffness matrix. However, since the element stiffness matrices can be constructed independent of each other, this process can be easily parallelized. Even without parallelization, this cost is negligible compared to the cost of solving the global set of equations, and, as already mentioned, this is considerably less in the case of hybrid elements due to the coarser meshes that are required to achieve a given level of accuracy.

Needless to say, the choice of the stress interpolation functions is critical in ensuring the accuracy of hybrid elements. Almost all works, such as [Punch and Atluri 1984; Lee and Rhiu 1986; Rhiu and Lee 1987], choose the stress interpolation function based on removal of spurious zero-energy modes so that the element stiffness matrix is full-rank (apart from rigid-body modes). It is well-known that the minimum number of stress-interpolation terms to ensure a full-rank element stiffness matrix is equal to the number of displacement degrees of freedom minus the number of rigid-body modes. It is also well known that adding more terms to the stress interpolation adds more stiffness. In the light of these two facts, efforts have naturally focused on keeping the number of stress interpolation terms to a minimum; henceforth, we will call such an interpolation with the minimum number of terms as a minimal stress interpolation. While such a strategy works extremely well for *static* problems, it was found recently in [Jog and Motamarri 2009] that it can result in instabilities on *transient* problems.

The cause of these problems is that the minimal stress interpolation in most (but not all) elements violates some basic tenets that interpolation functions should obey. To give a simple example, [Lee and Rhiu 1986; Rhiu and Lee 1987] discuss the interpolations for a 9-node quadrilateral element; the authors recommend dropping the term η^2 from the stress interpolation for the normal stress $\tau^{\xi\xi}$, where (ξ, η) denote the natural coordinates, since the kinematic mode which this term suppresses is non-communicable. Thus, the interpolation for $\tau^{\xi\xi}$ uses the set $\{1, \xi, \eta, \xi\eta, \xi\eta^2\}$, and in a similar manner, the interpolation for $\tau^{\eta\eta}$ uses the set $\{1, \xi, \eta, \xi\eta, \xi^2\eta\}$. Although the use of this interpolation yields excellent results on static problems, it results in instabilities on transient problems [Jog and Motamarri 2009]. The instabilities do not arise immediately (in fact, the results at small times match quite well with the expected results), but gradually creep in as the simulation progresses, and finally pollute the entire solution. The exclusion of η^2 and ξ^2 in the interpolations for $\tau^{\xi\xi}$ and $\tau^{\eta\eta}$ violates one of the basic principles that an interpolation function should obey, namely, that all terms *starting from the lowest and upto the highest order* should be included, and is the cause of the aforementioned instability. Another problem that commonly occurs in a minimal interpolation is that a β term is shared, or in other words, some stress components are coupled. As we will show, this can cause spurious stresses to arise even in static problems.

The focus of this work is to formulate a set of rules for the selection of the stress interpolation functions, so that problems of the type mentioned above do not occur, thus increasing the robustness of the resulting hybrid elements. Of course, adherence to these rules can result in an increase in the number of terms in the stress interpolation, and hence to a (slight) stiffening of the elements. But as we show by means

of several challenging examples (including nonlinear static and transient problems), the performance of the resulting hybrid elements continues to be far better than the displacement-based elements. To give an analogy, in a displacement-based formulation, reduced integration yields better results in many cases as compared to full integration, but can lead to spectacular failures as well. Thus, just as full integration results in elements that are stiffer but more robust, the rules enumerated here (which, besides the requirement that the element be free of spurious zero-energy modes, are based on some basic principles that interpolation functions should satisfy) result in stress interpolations with more terms than the minimal one for several elements, but are more robust in the sense that they do not result either in instabilities or in spurious stresses. We also mention that since we are usually using more terms than the mimimal one, the satisfaction of the inf-sup conditions [Xue et al. 1985] is not affected.

2. Choice of stress interpolation functions

In this section, we discuss the choice of stress interpolation functions for some three-dimensional hybrid elements in the light of our experience with static and transient simulations. If d is the number of displacement degrees of freedom, and r is the number of rigid body modes, then it is known that to obtain a formulation free of spurious energy modes, the number of chosen stress interpolation modes s must be at least $d-r$ [Punch and Atluri 1984]. As mentioned in the Introduction, since each additional mode adds more stiffness, an attempt is usually made to keep the number of stress modes to a minimum, i.e., $s=d-r$. However, it was shown in [Jog and Motamarri 2009] that some higher-order hybrid elements that satisfy this requirement, and are free of zero-energy modes, can still give rise to instabilities in transient problems. It was shown that if the normal stresses are obtained by differentiating the displacement field, then these instabilities do not arise. It is possible to interpolate the normal stresses in this manner, and such that the requirement $s=d-r$, and the requirement that the element matrix be free of spurious modes are still satisfied (see [Jog and Motamarri 2009] for examples). However, this involves dropping some of the lower-order terms in the shear interpolation, and this results in bad performance even on static problems. Thus, in order to obtain a robust element, one necessarily needs $s>d-r$ at least for some elements. Since static solutions can be considered as steady-state solutions to transient problems, one should use the same stress interpolations in static and transient simulations. To conclude, although using more stress modes than the minimal one does result in a slight stiffening, it is essential from the viewpoint of increased robustness of the element.

Based on this discussion, we propose the following set of rules (besides the obvious one that there be no spurious zero-energy modes) for choosing the stress interpolation functions in a hybrid formulation:

(1) The normal stress components should be obtained simply by differentiating the displacement interpolation functions. For example, in a three-dimensional hexahedral element, the interpolations for $\tau^{\xi\xi}$, $\tau^{\eta\eta}$ and $\tau^{\zeta\zeta}$ are obtained by differentiating the displacement interpolation functions with respect to ξ, η and ζ respectively.

(2) All the lower-order terms should be incorporated in the shear interpolation functions, e.g., a constant term in the case of a 8-node hexahedral element, or trilinear terms in the case of a 27-node hexahedral element. The higher-order terms in the shear interpolation are chosen so as to eliminate any spurious zero-energy modes, so that the element stiffness matrix is full-rank (apart from rigid-body modes). In addition, all the terms of the corresponding order of interpolation should also be

included (although they may not suppress any zero-energy mode). For example, in the case of the 27-node hexahedral element, only the higher-order terms $(\zeta^2\xi, \zeta^2\eta)$ are required in the interpolation for the shear component $S^{\xi\eta}$ to suppress the zero-energy modes. However, all the terms of the corresponding order (bilinear) of interpolation, namely $(\zeta^2, \zeta^2\xi, \zeta^2\eta, \zeta^2\xi\eta)$, should be included. Using an interpolation that violates this rule results in the transient algorithm diverging after a few time steps in the example discussed in Section 3H.

(3) The stress components should be allowed to vary independently of each other, i.e., there should be no shared β terms between stress components. This is especially important in problems involving either orthotropic materials where the three shear moduli G_{xy}, G_{yz} and G_{xz} could be different, or in materials with nonlinear constitutive relations where the shear stresses are not simply proportional to the corresponding shear strains. Not enforcing this requirement can result in spurious stresses even in linear problems, as we show below in the case of the 6-node wedge element.

(4) Finally, the stress interpolations should be such that the same results are obtained irrespective of the order of node-numbering in the connectivity specification. As we shall see, this requirement is difficult to satisfy in wedge elements.

We now discuss the choice of stress interpolation functions for several hybrid elements in the literature in the light of the rules above. Once the stress interpolation functions are chosen, the stiffness matrices are constructed as in [Jog and Kelkar 2006] and [Jog and Motamarri 2009] for the (nonlinear) static and transient cases, respectively. In what follows $\boldsymbol{S}$ denotes the second Piola-Kirchhoff stress tensor, while (u, v, w) denote the displacement components.

2A. ***Eight-node hexahedral element.*** We use the same interpolation for $\boldsymbol{S}$ as suggested by Pian and Tong [Pian and Tong 1986] in the context of linear problems, i.e.,

$$S^{\xi\xi} = \beta_1 + \beta_2\eta + \beta_3\zeta + \beta_4\eta\zeta, \quad S^{\eta\eta} = \beta_5 + \beta_6\xi + \beta_7\zeta + \beta_8\xi\zeta, \quad S^{\zeta\zeta} = \beta_9 + \beta_{10}\xi + \beta_{11}\eta + \beta_{12}\xi\eta,$$
$$S^{\xi\eta} = \beta_{13} + \beta_{14}\zeta, \quad S^{\eta\zeta} = \beta_{15} + \beta_{16}\xi, \quad S^{\xi\zeta} = \beta_{17} + \beta_{18}\eta.$$

This stress interpolation satisfies all the rules specified above. If the Jacobian matrix is given by

$$\boldsymbol{J} = \begin{bmatrix} \partial x/\partial\xi & \partial y/\partial\xi & \partial z/\partial\xi \\ \partial x/\partial\eta & \partial y/\partial\eta & \partial z/\partial\eta \\ \partial x/\partial\zeta & \partial y/\partial\zeta & \partial z/\partial\zeta \end{bmatrix} \equiv \begin{bmatrix} a_1 & b_1 & c_1 \\ a_2 & b_2 & c_2 \\ a_3 & b_3 & c_3 \end{bmatrix}, \tag{2-1}$$

then the transformation relation between the stress components expressed with respect to the natural and Cartesian coordinate systems is given by

$$\begin{bmatrix} S_{xx} \\ S_{yy} \\ S_{zz} \\ S_{xy} \\ S_{yz} \\ S_{xz} \end{bmatrix} = \boldsymbol{T} \begin{bmatrix} S^{\xi\xi} \\ S^{\eta\eta} \\ S^{\zeta\zeta} \\ S^{\xi\eta} \\ S^{\eta\zeta} \\ S^{\xi\zeta} \end{bmatrix}, \tag{2-2}$$

where

$$\boldsymbol{T} = \begin{bmatrix} a_1^2 & a_2^2 & a_3^2 & 2a_1a_2 & 2a_2a_3 & 2a_1a_3 \\ b_1^2 & b_2^2 & b_3^2 & 2b_1b_2 & 2b_2b_3 & 2b_1b_3 \\ c_1^2 & c_2^2 & c_3^2 & 2c_1c_2 & 2c_2c_3 & 2c_1c_3 \\ a_1b_1 & a_2b_2 & a_3b_3 & (a_2b_1+a_1b_2) & (a_2b_3+a_3b_2) & (a_1b_3+a_3b_1) \\ b_1c_1 & b_2c_2 & b_3c_3 & (b_2c_1+b_1c_2) & (b_2c_3+b_3c_2) & (b_1c_3+b_3c_1) \\ a_1c_1 & a_2c_2 & a_3c_3 & (a_1c_2+a_2c_1) & (a_3c_2+a_2c_3) & (a_3c_1+a_1c_3) \end{bmatrix}.$$

2B. ***Twenty-seven-node hexahedral element.*** We use the following "90β" interpolation:

$$\begin{aligned}
S^{\xi\xi} &= \beta_1 + \beta_2\xi + \beta_3\eta + \beta_4\zeta + \beta_5\xi\eta + \beta_6\eta\zeta + \beta_7\xi\zeta + \beta_8\xi\eta\zeta \\
&\quad + \beta_9\xi\eta^2 + \beta_{10}\xi\zeta^2 + \beta_{11}\xi\eta\zeta^2 + \beta_{12}\xi\eta^2\zeta + \beta_{13}\xi\eta^2\zeta^2 \\
&\quad + \beta_{14}\eta^2 + \beta_{15}\zeta^2 + \beta_{16}\eta^2\zeta + \beta_{17}\eta\zeta^2 + \beta_{18}\eta^2\zeta^2, \\
S^{\eta\eta} &= \beta_{19} + \beta_{20}\xi + \beta_{21}\eta + \beta_{22}\zeta + \beta_{23}\xi\eta + \beta_{24}\eta\zeta + \beta_{25}\xi\zeta + \beta_{26}\xi\eta\zeta \\
&\quad + \beta_{27}\xi^2\eta + \beta_{28}\eta\zeta^2 + \beta_{29}\xi^2\eta\zeta + \beta_{30}\xi\eta\zeta^2 + \beta_{31}\xi^2\eta\zeta^2 \\
&\quad + \beta_{32}\xi^2 + \beta_{33}\zeta^2 + \beta_{34}\xi^2\zeta + \beta_{35}\xi\zeta^2 + \beta_{36}\xi^2\zeta^2, \\
S^{\zeta\zeta} &= \beta_{37} + \beta_{38}\xi + \beta_{39}\eta + \beta_{40}\zeta + \beta_{41}\xi\eta + \beta_{42}\eta\zeta + \beta_{43}\xi\zeta + \beta_{44}\xi\eta\zeta \\
&\quad + \beta_{45}\xi^2\zeta + \beta_{46}\eta^2\zeta + \beta_{47}\xi^2\eta\zeta + \beta_{48}\xi\eta^2\zeta + \beta_{49}\xi^2\eta^2\zeta \\
&\quad + \beta_{50}\xi^2 + \beta_{51}\eta^2 + \beta_{52}\xi^2\eta + \beta_{53}\xi\eta^2 + \beta_{54}\xi^2\eta^2, \\
S^{\xi\eta} &= \beta_{55} + \beta_{56}\xi + \beta_{57}\eta + \beta_{58}\zeta + \beta_{59}\xi\eta + \beta_{60}\eta\zeta + \beta_{61}\xi\zeta + \beta_{62}\xi\eta\zeta \\
&\quad + \beta_{63}\xi\zeta^2 + \beta_{64}\eta\zeta^2 + \beta_{85}\zeta^2 + \beta_{88}\zeta^2\xi\eta, \\
S^{\eta\zeta} &= \beta_{65} + \beta_{66}\xi + \beta_{67}\eta + \beta_{68}\zeta + \beta_{69}\xi\eta + \beta_{70}\eta\zeta + \beta_{71}\xi\zeta + \beta_{72}\xi\eta\zeta \\
&\quad + \beta_{73}\xi^2\eta + \beta_{74}\xi^2\zeta + \beta_{86}\xi^2 + \beta_{89}\xi^2\eta\zeta, \\
S^{\xi\zeta} &= \beta_{75} + \beta_{76}\xi + \beta_{77}\eta + \beta_{78}\zeta + \beta_{79}\xi\eta + \beta_{80}\eta\zeta + \beta_{81}\xi\zeta + \beta_{82}\xi\eta\zeta \\
&\quad + \beta_{83}\xi\eta^2 + \beta_{84}\eta^2\zeta + \beta_{87}\eta^2 + \beta_{90}\xi\eta^2\zeta.
\end{aligned} \tag{2-3}$$

The transformation to Cartesian components is carried out using (2-2).

The minimum number of interpolation terms required for this element is 75, and indeed such an interpolation was developed in [Jog 2005] within a linear context. However, such an interpolation violates Rules (1) and (3), and results in instabilities in some transient problems [Jog and Motamarri 2009]. Thus, increased robustness necessitates using the 90β element above, although it is stiffer compared to the 75β element (but note that it is still more flexible compared to the 8-node hexahedral element for a given number of degrees of freedom). As per Rule (1), one constructs the interpolation for the normal stresses simply by differentiating the displacement interpolation functions. To construct the shear-interpolation, one first includes all the lower-order (i.e., trilinear) terms. Among the higher-order terms, the (β_{63}, β_{64}), (β_{73}, β_{74}) and (β_{83}, β_{84}) terms are included to suppress the zero-energy modes

$$\begin{aligned}
&u = \alpha_1(1-3\eta^2)(1-3\zeta^2),\ \ v = 0,\ \ w = 0; \\
&u = 0,\ \ v = \alpha_2(1-3\xi^2)(1-3\zeta^2),\ \ w = 0; \\
&u = 0,\ \ v = 0,\ \ w = \alpha_3(1-3\xi^2)(1-3\eta^2).
\end{aligned}$$

These modes can be suppressed by using only three β terms. However, this would violate Rule (3) that the stress components be allowed to vary independently. The β_{85}–β_{90} terms are included to comply with Rule (2). According to this rule, along with the terms $\zeta^2\xi$ and $\zeta^2\eta$ which are required to suppress the zero-energy modes in $S^{\xi\eta}$, one should also include the terms ζ^2 and $\zeta^2\xi\eta$; thus, the terms in the interpolation for $S^{\xi\eta}$ that one finally obtains are given by products of the set $\{1, \xi, \eta, \xi\eta\}$ with the set $\{1, \zeta, \zeta^2\}$. Note that in both the 8-node and 27-node hexahedral elements, the terms in the final interpolations for the shear stresses S^{ij} are the terms that are common in the interpolations for the normal stresses S^{ii} and S^{jj}.

2C. ***Six-node wedge element.*** The requirement imposed by Rule (4) is difficult to satisfy in the case of wedge elements. In particular, if one formulates the stress modes in terms of natural coordinates as in the case of hexahedral elements, *and* if one uses the minimum number of stress modes, then this requirement is violated. To overcome this problem, Sze et al. [Sze et al. 2004a] proposed a novel idea of using a local Cartesian system to express the stress interpolation functions. Their proposed interpolation with respect to this local Cartesian system x'-y'-z' is

$$\begin{aligned} &S_{x'x'} = \beta_1 + \beta_2\zeta, \quad S_{y'y'} = \beta_3 + \beta_4\zeta, \qquad S_{z'z'} = \beta_5 + \beta_6\xi + \beta_7\eta, \\ &S_{x'y'} = \beta_8 + \beta_9\zeta, \quad S_{y'z'} = \beta_{10} + \beta_{12}x', \quad S_{x'z'} = \beta_{11} - \beta_{12}y'. \end{aligned}$$

Quite unfortunately, it violates the requirement that the stresses be allowed to vary independently of each other since β_{12} is shared between $S_{y'z'}$ and $S_{x'z'}$. If one considers a single element, with the local and global coordinate systems coinciding, then the displacement field $u = 0$, $v = xz$, $w = 0$, within a linear context, yields $S_{yz} = Gx$, $S_{xz} = 0$, while the numerical strategy yields a nonzero S_{xz} due to its coupling with S_{yz}; thus, using a shared β results in a spurious S_{xz} component. One would surmise that the situation can be corrected by using

$$\begin{aligned} &S_{x'x'} = \beta_1 + \beta_2\zeta, \quad S_{y'y'} = \beta_3 + \beta_4\zeta, \qquad S_{z'z'} = \beta_5 + \beta_6\xi + \beta_7\eta, \\ &S_{x'y'} = \beta_8 + \beta_9\zeta, \quad S_{y'z'} = \beta_{10} + \beta_{12}x', \quad S_{x'z'} = \beta_{11} + \beta_{13}y'. \end{aligned}$$

However, numerical experiments show that such an interpolation fails to converge on the (nonlinear) pinched hemisphere problem even with the use of a large number of load steps.

Hence, we finally use the following interpolation which, similar to hexahedral elements, uses the natural coordinate system:

$$\begin{aligned} &S^{\xi\xi} = \beta_1 + \beta_2\zeta, \quad S^{\eta\eta} = \beta_3 + \beta_4\zeta, \qquad S^{\zeta\zeta} = \beta_5 + \beta_6\xi + \beta_7\eta, \\ &S^{\xi\eta} = \beta_8 + \beta_9\zeta, \quad S^{\eta\zeta} = \beta_{10} + \beta_{11}\xi + \beta_{12}\eta, \quad S^{\xi\zeta} = \beta_{13} + \beta_{14}\xi + \beta_{15}\eta. \end{aligned}$$

The transformation to Cartesian components is carried out using (2-2). Since the $S^{\eta\zeta}$ and $S^{\xi\eta}$ components use interpolations that are symmetric in ξ and η, Rule (4) is satisfied.

Once again, we see that compliance with the 4 requirements results in an element with higher number of β's than the minimum, which is 12. Numerical experiments show that this element is only marginally better than the displacement-based 6-node wedge element.

2D. ***Eighteen-node wedge element.*** The displacement shape functions are obtained as the product of the standard 6-node (quadratic) triangle shape functions with the quadratic one-dimensional shape functions.

The stress interpolation functions are

$$\begin{aligned}
S^{\xi\xi} &= \beta_1 + \beta_2\xi + \beta_3\eta + \beta_4\zeta + \beta_5\xi\zeta + \beta_6\eta\zeta + \beta_7\zeta^2 + \beta_8\xi\zeta^2 + \beta_9\eta\zeta^2,\\
S^{\eta\eta} &= \beta_{10} + \beta_{11}\xi + \beta_{12}\eta + \beta_{13}\zeta + \beta_{14}\xi\zeta + \beta_{15}\eta\zeta + \beta_{16}\zeta^2 + \beta_{17}\xi\zeta^2 + \beta_{18}\eta\zeta^2,\\
S^{\zeta\zeta} &= \beta_{19} + \beta_{20}\xi + \beta_{21}\eta + \beta_{22}\xi^2 + \beta_{23}\xi\eta + \beta_{24}\eta^2 + \beta_{25}\zeta\\
&\quad + \beta_{26}\xi\zeta + \beta_{27}\eta\zeta + \beta_{28}\xi^2\zeta + \beta_{29}\eta^2\zeta + \beta_{30}\xi\eta\zeta,\\
S^{\xi\eta} &= \beta_{31} + \beta_{32}\xi + \beta_{33}\eta + \beta_{34}\zeta + \beta_{35}\xi\zeta + \beta_{36}\eta\zeta + \beta_{37}\zeta^2 + \beta_{38}\xi\zeta^2 + \beta_{39}\eta\zeta^2,\\
S^{\eta\zeta} &= \beta_{40} + \beta_{41}\xi + \beta_{42}\eta + \beta_{43}\zeta + \beta_{44}\xi\zeta + \beta_{45}\eta\zeta,\\
S^{\xi\zeta} &= \beta_{46} + \beta_{47}\xi + \beta_{48}\eta + \beta_{49}\zeta + \beta_{50}\xi\zeta + \beta_{51}\eta\zeta.
\end{aligned} \tag{2-4}$$

The transformation to Cartesian components is carried out using (2-2). An 18-point (6×3) Gauss quadrature rule is used to carry out the integrations.

Notes. • Removing the β_{37} term does not affect the rank of the element stiffness matrix (or, in other words, this term does not suppress any zero energy modes). But excluding this term violates Rules (2) and (4); i.e., the results become sensitive to the order of numbering in the connectivity list. Thus, again, a slightly higher number of stress functions than the minimum are required to ensure robustness.

• Numerical experiments show that although the 21-node wedge element of [Jog 2005] performs slightly better than the above 18-node wedge element on coarser meshes, the convergence of the latter element with mesh refinement is more rapid. The reason is that derivatives of the bubble function introduced in the 21-node element formulation are part of the shear interpolation shape functions, which tends to make the 21-node stiffness matrix overstiff, especially in plate or shell structures. The development of the 18-node wedge element is also simpler because there is no bubble function — no local Cartesian system needs to be introduced as in the 21-node element to ensure insensitivity to node numbering.

• Even from a mesh-generation viewpoint, using the 18-node wedge element is advantageous since it is a standard element that is offered by many meshing softwares.

2E. ***Tetrahedral elements.*** Since meshing is far easier with tetrahedral elements than with hexahedral elements, the question naturally arises if tetrahedral elements can be improved using the hybrid element methodology. Since the shape functions of the 4-node linear and 10-node quadratic tetrahedral elements involve complete polynomials, the displacement-based and hybrid methodologies yield identical results for these elements. Lo and Ling [2000] suggested an improvement for the 10-node tetrahedral element based on an incompatible displacement field. Here, we shall investigate if an improvement in this element is possible by introducing a bubble mode associated with a node in the interior (say, at the centroid) of this element. Thus, let ξ, η, ζ be the standard volume coordinates, let $\alpha = 1-\xi-\eta-\zeta$, and let $N_b = \xi\eta\zeta\alpha$ be the bubble mode associated with the eleventh node. The displacement shape functions are now

$$\begin{aligned}
N_1 &= \xi(2\xi-1) + 32N_b, & N_5 &= 4\xi\eta - 64N_b, & N_9 &= 4\eta\alpha - 64N_b,\\
N_2 &= \eta(2\eta-1) + 32N_b, & N_6 &= 4\eta\zeta - 64N_b, & N_{10} &= 4\zeta\alpha - 64N_b,\\
N_3 &= \zeta(2\zeta-1) + 32N_b, & N_7 &= 4\xi\zeta - 64N_b, & N_{11} &= 256N_b.\\
N_4 &= \alpha(2\alpha-1) + 32N_b, & N_8 &= 4\xi\alpha - 64N_b,
\end{aligned}$$

The stress shape functions can be formulated directly with respect to the global Cartesian system as

$$\begin{aligned}
S_{xx} &= \beta_1 + \beta_7\xi + \beta_{13}\eta + \beta_{19}\zeta + \beta_{25}\,\partial N_b/\partial x,\\
S_{yy} &= \beta_2 + \beta_8\xi + \beta_{14}\eta + \beta_{20}\zeta + \beta_{26}\,\partial N_b/\partial y,\\
S_{zz} &= \beta_3 + \beta_9\xi + \beta_{15}\eta + \beta_{21}\zeta + \beta_{27}\,\partial N_b/\partial z,\\
S_{xy} &= \beta_4 + \beta_{10}\xi + \beta_{16}\eta + \beta_{22}\zeta,\\
S_{yz} &= \beta_5 + \beta_{11}\xi + \beta_{17}\eta + \beta_{23}\zeta,\\
S_{xz} &= \beta_6 + \beta_{12}\xi + \beta_{18}\eta + \beta_{24}\zeta,
\end{aligned}$$

where, with $\boldsymbol{J}$ given by (2-1), we have

$$\begin{bmatrix} \partial N_b/\partial x \\ \partial N_b/\partial y \\ \partial N_b/\partial z \end{bmatrix} = \boldsymbol{J}^{-1} \begin{bmatrix} \partial N_b/\partial \xi \\ \partial N_b/\partial \eta \\ \partial N_b/\partial \zeta \end{bmatrix}.$$

Unfortunately, the improvement of the 11-node hybrid element over the displacement-based 10-node tetrahedral element is marginal, so it is preferable simply to use the 10-node displacement-based element.

2F. ***Four-node axisymmetric element.*** With the Jacobian matrix given by

$$\boldsymbol{J} = \begin{bmatrix} \partial r/\partial \xi & \partial z/\partial \xi \\ \partial r/\partial \eta & \partial z/\partial \eta \end{bmatrix},$$

we use the same shape functions for $\boldsymbol{S}$ as developed in [Jog and Annabatula 2006] for linear problems, namely,

$$\begin{bmatrix} S_{rr} \\ S_{zz} \\ S_{rz} \end{bmatrix} = \begin{bmatrix} J_{11}^2 & J_{21}^2 & 2J_{11}J_{21} \\ J_{12}^2 & J_{22}^2 & 2J_{12}J_{22} \\ J_{11}J_{12} & J_{21}J_{22} & J_{11}J_{22} + J_{12}J_{21} \end{bmatrix} \begin{bmatrix} S^{\xi\xi} \\ S^{\eta\eta} \\ S^{\xi\eta} \end{bmatrix} \quad \text{and} \quad S_{\theta\theta} = \beta_6 + \beta_7(J_{12}\xi + J_{22}\eta),$$

where

$$S^{\xi\xi} = \beta_1 + \beta_4\eta, \quad S^{\eta\eta} = \beta_2 + \beta_5\xi, \quad S^{\xi\eta} = \beta_3.$$

2G. ***Nine-node axisymmetric element.*** With the Jacobian matrix as in the case of the 4-node axisymmetric element, the shape functions are given by

$$\begin{bmatrix} S_{rr} \\ S_{zz} \\ S_{rz} \end{bmatrix} = \begin{bmatrix} J_{11}^2 & J_{21}^2 & 2J_{11}J_{21} \\ J_{12}^2 & J_{22}^2 & 2J_{12}J_{22} \\ J_{11}J_{12} & J_{21}J_{22} & J_{11}J_{22} + J_{12}J_{21} \end{bmatrix} \begin{bmatrix} S^{\xi\xi} \\ S^{\eta\eta} \\ S^{\xi\eta} \end{bmatrix}$$

and

$$S_{\theta\theta} = \beta_{17} + \beta_{18}\xi + \beta_{19}\eta + \beta_{20}\xi\eta + \beta_{21}\xi^2 + \beta_{22}\eta^2 + \beta_{23}(J_{12}\xi^2\eta + J_{22}\xi\eta^2),$$

where

$$\begin{aligned}
S^{\xi\xi} &= \beta_1 + \beta_2\xi + \beta_3\eta + \beta_4\xi\eta + \beta_5\eta^2 + \beta_6\xi\eta^2,\\
S^{\eta\eta} &= \beta_7 + \beta_8\xi + \beta_9\eta + \beta_{10}\xi\eta + \beta_{11}\xi^2 + \beta_{12}\xi^2\eta,\\
S^{\xi\eta} &= \beta_{13} + \beta_{14}\xi + \beta_{15}\eta + \beta_{16}\xi\eta.
\end{aligned}$$

The higher-order terms in $S_{\theta\theta}$ are chosen to be of the same order as S_{rr}. Although excluding them would still ensure a full-rank stiffness matrix (modulo the rigid-body mode), including them ensures that one gets an almost symmetrical solution in the thick sphere problem of Section 3F.

3. Numerical examples

In this section, we present several linear and nonlinear example problems, both static and transient, to demonstrate the good performance of the hybrid elements. The displacement-based and hybrid n-noded (where n is either 8 or 27) brick elements are denoted by Bn and Sn respectively, the displacement-based and hybrid n-noded wedge elements (where n is either 6 or 18) are denoted by Bn and Wn respectively, while the displacement-based and hybrid n-noded (where n is either 4 or 9) axisymmetric elements are denoted by Bn and An respectively. The WSMP sparse matrix solver [Gupta 2000; 2002] is used. Full integration is used to construct the element stiffness matrices in all cases. We use the expressions given by Equation (30) of [Jog and Kelkar 2006] to compute the stiffness and load vectors in the case of pressure loading for both the displacement-based and hybrid elements. For axisymmetric problems, with 1, 2 and 3 denoting the r, z and θ directions, the matrix $\boldsymbol{R}$ and vector $(\mathbf{cof}\,\boldsymbol{F})\tilde{\boldsymbol{n}}^0$ in these expressions are

$$\boldsymbol{R}^k = \begin{bmatrix} 0 & 0 & -F^k_{33}\tilde{n}^0_2 & F^k_{33}\tilde{n}^0_1 & F^k_{22}\tilde{n}^0_1 - F^k_{21}\tilde{n}^0_2 \\ F^k_{33}\tilde{n}^0_2 & -F^k_{33}\tilde{n}^0_1 & 0 & 0 & F^k_{11}\tilde{n}^0_2 - F^k_{12}\tilde{n}^0_1 \end{bmatrix}, \quad (\mathbf{cof}\,\boldsymbol{F}^k)\tilde{\boldsymbol{n}}^0 = \begin{bmatrix} F^k_{22}F^k_{33}\tilde{n}^0_1 - F^k_{21}F^k_{33}\tilde{n}^0_2 \\ -F^k_{12}F^k_{33}\tilde{n}^0_1 + F^k_{11}F^k_{33}\tilde{n}^0_2 \end{bmatrix},$$

where $(\tilde{n}^0_1, \tilde{n}^0_2) = (\partial z/\partial\xi, -\partial r/\partial\xi)$ denotes the normal in the reference configuration, and k denotes the iteration number.

As in [Jog and Kelkar 2006], to ensure a fair comparison of the results, meshes with the *same number of global degrees of freedom* are used; e.g., on any given problem involving hexahedral elements, results obtained using $8N$ eight-node brick elements are compared with those obtained using N twenty-seven-node brick elements, with identical nodal coordinate data and boundary conditions used in both meshes. In all problems, uniform meshes are used. In the case of the hybrid elements, the nodal stresses are obtained by finding the nodal values in each element using the stress interpolation and then averaging, while in the case of the displacement-based elements, the stresses are found by extrapolating the values from the Gauss points, followed by averaging. A Saint Venant–Kirchhoff material model (default) or a neo-Hookean material model with strain energy density and constitutive relation either given by

$$\begin{aligned} W(\boldsymbol{C}) &= \tfrac{1}{8}\lambda(\log\det\boldsymbol{C})^2 + \tfrac{1}{2}\mu(\operatorname{tr}\boldsymbol{C} - 3 - \log\det\boldsymbol{C}), \\ \boldsymbol{S}(\boldsymbol{C}) &= 2\frac{\partial W}{\partial \boldsymbol{C}} = \frac{\lambda}{2}(\log\det\boldsymbol{C})\boldsymbol{C}^{-1} + \mu(\boldsymbol{I} - \boldsymbol{C}^{-1}), \end{aligned} \tag{3-1}$$

or by

$$\begin{aligned} W(\boldsymbol{C}) &= c_1(\bar{I}_1 - 3) + \tfrac{1}{2}\kappa(J-1)^2, \\ \boldsymbol{S}(\boldsymbol{C}) &= \left(-\tfrac{2}{3}c_1 I_1 I_3^{-1/3} + \kappa(I_3 - I_3^{1/2})\right)\boldsymbol{C}^{-1} + 2c_1 I_3^{-1/3}\boldsymbol{I}, \end{aligned} \tag{3-2}$$

where $\boldsymbol{C} = \boldsymbol{F}^T\boldsymbol{F}$, $I_1 = \operatorname{tr}\boldsymbol{C}$, $I_3 = \det\boldsymbol{C}$, $\bar{I}_1 = (I_3)^{-1/3}I_1$, and $\kappa = \lambda + 2\mu/3$ is the bulk modulus, is used in all the examples (the strains are recovered from the stresses as outlined in [Jog and Kelkar 2006]). Typically, on all the static nonlinear shell-type problems presented, convergence is achieved in

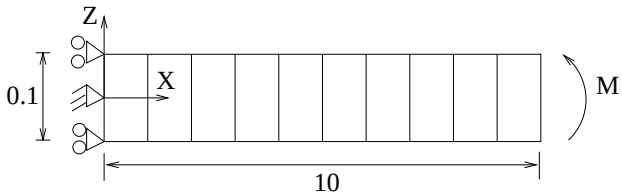

Figure 1. Rollup of a beam. The beam is shown discretized using ten 27-node elements.

about a tenth of the number of iterations reported in [Sze et al. 2004b]. As expected, the results obtained using the proposed hybrid elements are slightly stiffer compared to results obtained using elements with minimal stress interpolations. This is the cost for the increased robustness; however, as we show, the performance is still much better compared to displacement-based elements.

3A. ***Roll-up of a beam (elastica problem).*** An initially flat shell of length $L = 10$, width $w = 1$ and thickness $t = 0.1$ is subjected to a bending moment as shown in Figure 1. The moment is applied through a linearly varying distributed traction on the right face. The material properties are $E = 12 \times 10^6$ and $\nu = 0$. The *shell* solution for the tip displacements of the midsurface is

$$u = R \sin \frac{X}{R}, \quad v = 0, \quad w = R\left(1 - \cos \frac{X}{R}\right), \tag{3-3}$$

where $R = EI/M$ is the radius of curvature. For $M = 2\pi EI/L$, the beam rolls up into a complete circle. We apply the linearly varying traction corresponding to this value of the moment; note that, since this traction remains normal to the surface as the beam deforms, we have to consider the loading as deformation dependent. The deformed shapes obtained using the S27 and B27 elements, obtained using approximately a total of 60 and 90 iterations, respectively, are shown in Figure 2, and should be compared with the solution in Figure 4 of [Jog and Kelkar 2006], which was obtained using the minimum number of stress interpolation terms, namely 75. It is evident from this figure that the 90β interpolation used in this work does not result in any additional stiffening compared to the 75β interpolation, and continues to perform much better compared to the displacement-based element which not only locks, but also takes more number of iterations to converge. The small deviation from the exact solution seen in the S27 element results could be because the load is not being applied in a manner consistent with the three-dimensional exact solution (since this exact solution is not known), but rather in an approximate

Figure 2. Deformed geometries for the elastica problem obtained using the S27 (left) and the B27 (right) elements.

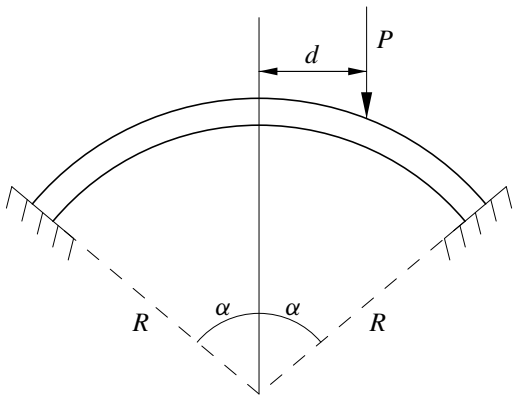

Figure 3. Shallow spherical cap subjected to an asymmetric point load P.

way. Sze et al. [2004b] report having to use more than 700 iterations to solve this problem using shell elements from a commercial software.

3B. ***Shallow spherical cap subjected to an asymmetric point load.*** This example was solved in [Danielson and Tielking 1993] using Fourier elements. The setup is shown in Figure 3. The geometric parameters shown are $R = 4.76\,\text{in}$, $d = 0.328\,\text{in}$ and $\alpha = 10.9°$, and the thickness is $0.01576\,\text{in}$. The material parameters are $E = 10^7$ psi and $\nu = 0.3$. Meshes $n_R \times n_\alpha \times n_\phi$ of $1 \times 7 \times 8$ and $2 \times 14 \times 16$ of higher and lower-order wedge/hexahedral elements are used to discretize the structure. Wedge elements are used in the layer closest to the apex, and hexahedral elements are used elsewhere. The load-deflection curves for the displacement at the apex and under the point load are shown in Figure 4, and should be compared with Danielson and Tielking's Figures 8 and 9. The number of iterations required to converge at each load step is about 4 or 5. As mentioned in their article, this problem is challenging because the shell almost buckles as it folds through: the final deflection at $P = 60\,\text{lb}$ is more than an order of magnitude greater than the linear solution.

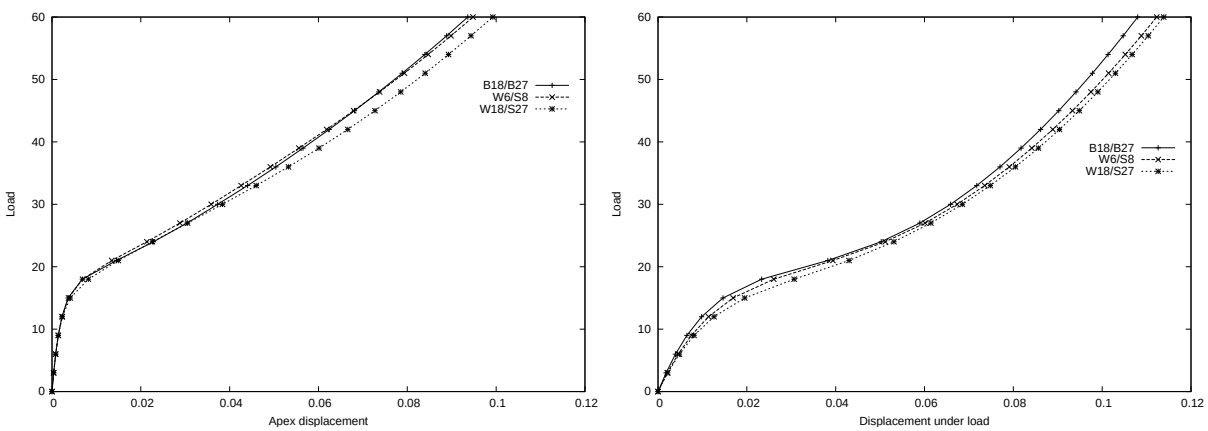

Figure 4. Load deflection curves for apex and loading point for the shallow spherical cap problem.

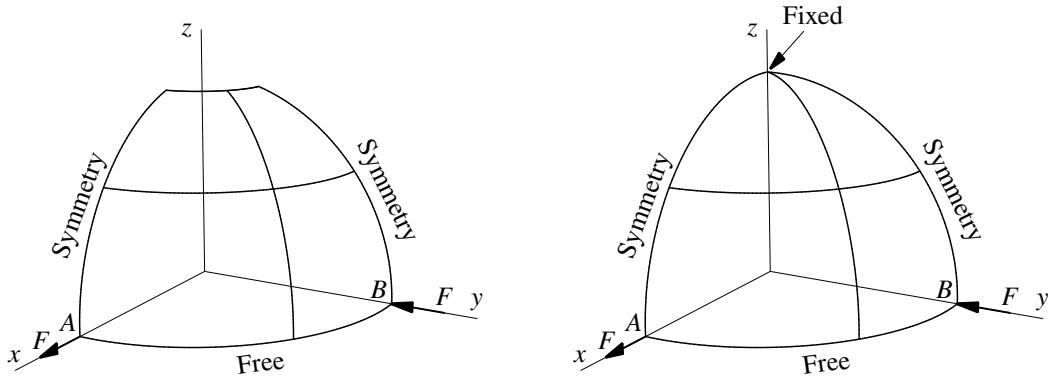

Figure 5. Pinched hemispherical shell with and without an 18° hole; only a quadrant is modelled in both problems due to symmetry.

3C. ***Hemispherical shell subjected to alternating radial loads.*** A hemisphere with and without an 18° hole at the top is subjected to pinching loads; only a quadrant is modelled due to symmetry as shown in Figure 5 with $F = 1$ and $F = 200$ for the linear and nonlinear cases respectively. The properties are $E = 6.825 \times 10^7$, $\nu = 0.3$, mean radius $R = 10$, and thickness $h = 0.04$. Meshes of $4 \times 4 \times 2$, $8 \times 8 \times 2$ and $16 \times 16 \times 2$ eight-node brick elements, and $2 \times 2 \times 1$, $4 \times 4 \times 1$ and $8 \times 8 \times 1$ twenty-seven-node brick elements are used in the case where the hemisphere has a hole; meshes with the same number of nodes per side are used for the full hemisphere case, with the layer around to the pole being modelled by wedge elements. For the linear case, the results for the displacement at the point of application of the forces, normalized against the solutions of 0.09355 and 0.0924, are presented in Table 1.

For the nonlinear case, the reference solutions for the displacements at points A and B are 4.067 and 8.178 in the case of the hemisphere with a hole, and 4.0754 and 8.1449 in the case of the hemisphere without a hole [Sze et al. 2004b]. The normalized results are presented in Table 2. The solutions in all

	Hemisphere with hole			Hemisphere without hole		
Nodes/side	B27	S8	S27	B18/B27	W6/S8	W18/S27
5	0.00146	0.0896	0.5879	0.00109	0.0186	0.0437
9	0.02174	0.8645	0.9514	0.01157	0.4120	0.7846
17	0.25715	0.9942	0.9892	0.19478	0.9561	0.9849

Table 1. Normalized displacements for the pinched hemisphere problem: linear case.

Nodes per side	Hemisphere with hole						Hemisphere without hole					
	Point A			Point B			Point A			Point B		
	B27	S8	S27	B27	S8	S27	B18/B27	W6/S8	W18/S27	B18/B27	W6/S8	W18/S27
5	.00669	.30582	.59848	.00334	.20494	.58447	.00494	.08113	.14896	.00267	.04395	.16284
9	.09463	.76729	.82610	.05130	.70661	.76408	.06869	.67206	.79258	.03619	.57386	.72805
17	.50568	.94674	.96256	.37750	.93283	.94663	.45291	.93293	.95312	.30843	.91480	.93710

Table 2. Normalized displacements for the pinched hemisphere problem: nonlinear case.

cases are obtained using a single load step, and the number of iterations is approximately 9 for the hybrid elements, while with the use of the finest mesh, the number of iterations required for the two problems with the displacement-based approach is 21 and 18 respectively.

3D. ***Thick and thin shell subjected to line loading.*** This example has been solved in [Reese et al. 2000] using an enhanced strain method. A hollow cylindrical shell of mean radius 9 mm is simply supported at its bottom, and subjected to a uniform line load q at the top as shown in Figure 6. Two cases are considered: (i) a moderately thick shell with $t = 2$ mm and $q = 500\,\text{N/mm}$, and (ii) a thin shell with $t = 0.2$ mm and $q = 8.5/15\,\text{N/mm}$. As in that reference, only a quarter of the domain is modelled by using meshes $n_r \times n_\theta \times n_z$ of $1 \times 8 \times 4$, $1 \times 16 \times 8$ and $1 \times 32 \times 16$ 27-node hexahedral elements, and $2 \times 16 \times 8$, $2 \times 32 \times 16$ and $2 \times 64 \times 32$ 8-node hexahedral elements. The material model used is the compressible neo-Hookean model given by (3-1) with $\lambda = 24000\ \text{N/mm}^2$ and $\mu = 6000\ \text{N/mm}^2$ (the value of λ is stated as $240000\ \text{N/mm}^2$ in [Reese et al. 2000] due to a typographical error). The variation of the vertical displacement at A with mesh refinement for the thick and thin shells is shown in Figure 7, and should be compared with Reese's Figure 2.

As can be seen, the displacement-based elements lock severely in the thin shell case, despite our use of a higher-order element. The number of iterations is also substantially more for the displacement-based

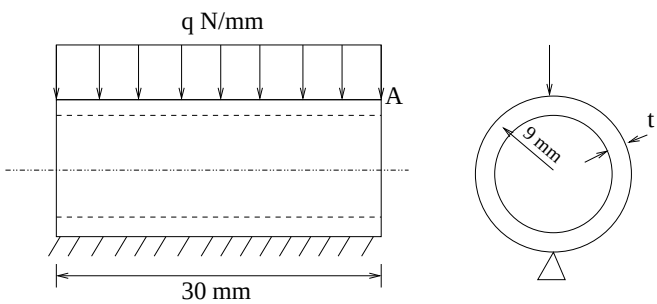

Figure 6. Hollow cylinder subjected to line loading. Only a quarter of the domain is modelled due to symmetry.

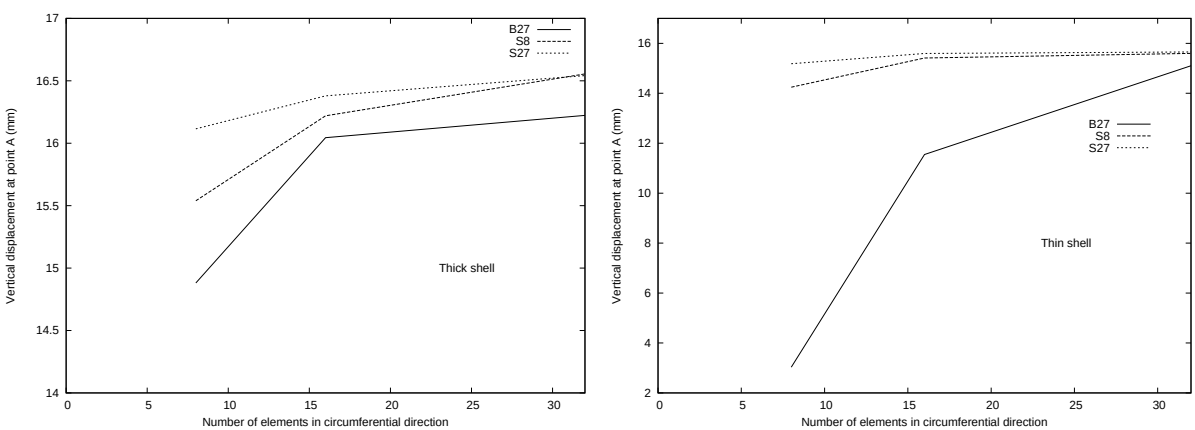

Figure 7. Convergence study for the thick and thin shell examples.

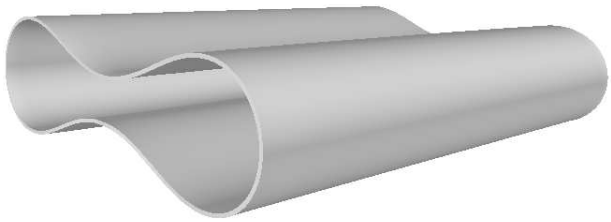

Figure 8. Deformed shape of the thin shell subjected to line load.

elements. Although the performance of the lower-order hybrid elements is slightly poorer compared to their corresponding higher-order hybrid counterparts on coarse meshes, they converge very rapidly with mesh refinement as seen from Figure 7; this is a trend observed in all the examples where a lower-order hybrid element yields slightly poorer results compared to its higher-order counterpart on a coarse mesh. For both the thick and thin shell cases, convergence for both the 8-node and 27-node hexahedral elements is achieved in a single load step and approximately 8 iterations. In contrast, with the finest mesh of B27 elements, convergence is achieved in 5 load steps and a total of 34 iterations for the thick shell case, and 20 load steps and a total of 120 iterations for the thin shell case! To give an idea of the extreme deformation involved in this problem, the deformed shape of the thin shell is shown in Figure 8.

3E. ***Elastic wave propagation in a circular disk.*** A part of one face of a circular disk is subjected to an axisymmetric pressure loading while the remainder of the boundary is free of tractions as shown in Figure 9; compare [Cherukuri and Shawki 1996]. The parameters used are $H = 1$, $R = 1.5$, $r_p = 0.25$, $t_1 = 2\,\mu$s, $t_2 = 5\,\mu$s, $t_3 = 7\,\mu$s, $P = 10^5$, while the material properties are $E = 9.1 \times 10^6$, $\nu = 0.2$ and $\rho = 2.0835 \times 10^{-4}$. A uniform mesh $n_r \times n_z$ of 30×20 A9 elements is used to discretize the domain, and the time step used is $t_\Delta = 0.1\,\mu$s. The energy-momentum conserving algorithm of [Jog and Motamarri 2009] is used to advance the solution in time. As opposed to the conditionally stable algorithm in [Cherukuri and Shawki 1996], our time-stepping strategy is unconditionally stable, allowing one to take larger time steps. As noted in this reference, the time required for a longitudinal wave to traverse the thickness once is approximately $4.54\,\mu$s. During the time of interest ($60\,\mu$s), multiple reflections take place, and consequently the numerical strategy should be sufficiently robust to accurately predict the displacements during and after these reflections.

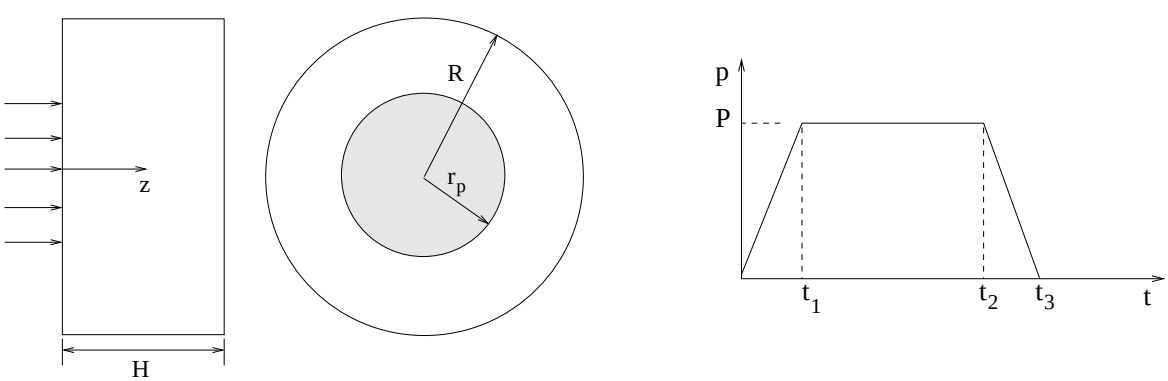

Figure 9. Elastic wave propagation in a circular disk.

The radial and axial displacements obtained using the A9 element are shown in the top two graphs of Figure 10; these should be compared with Figures 10 and 11 of [Cherukuri and Shawki 1996]. Similarly, the radial, longitudinal, shear and hoop stresses are shown in the remaining graphs of Figure 10, which should be compared with Figures 12–15 of the same reference.

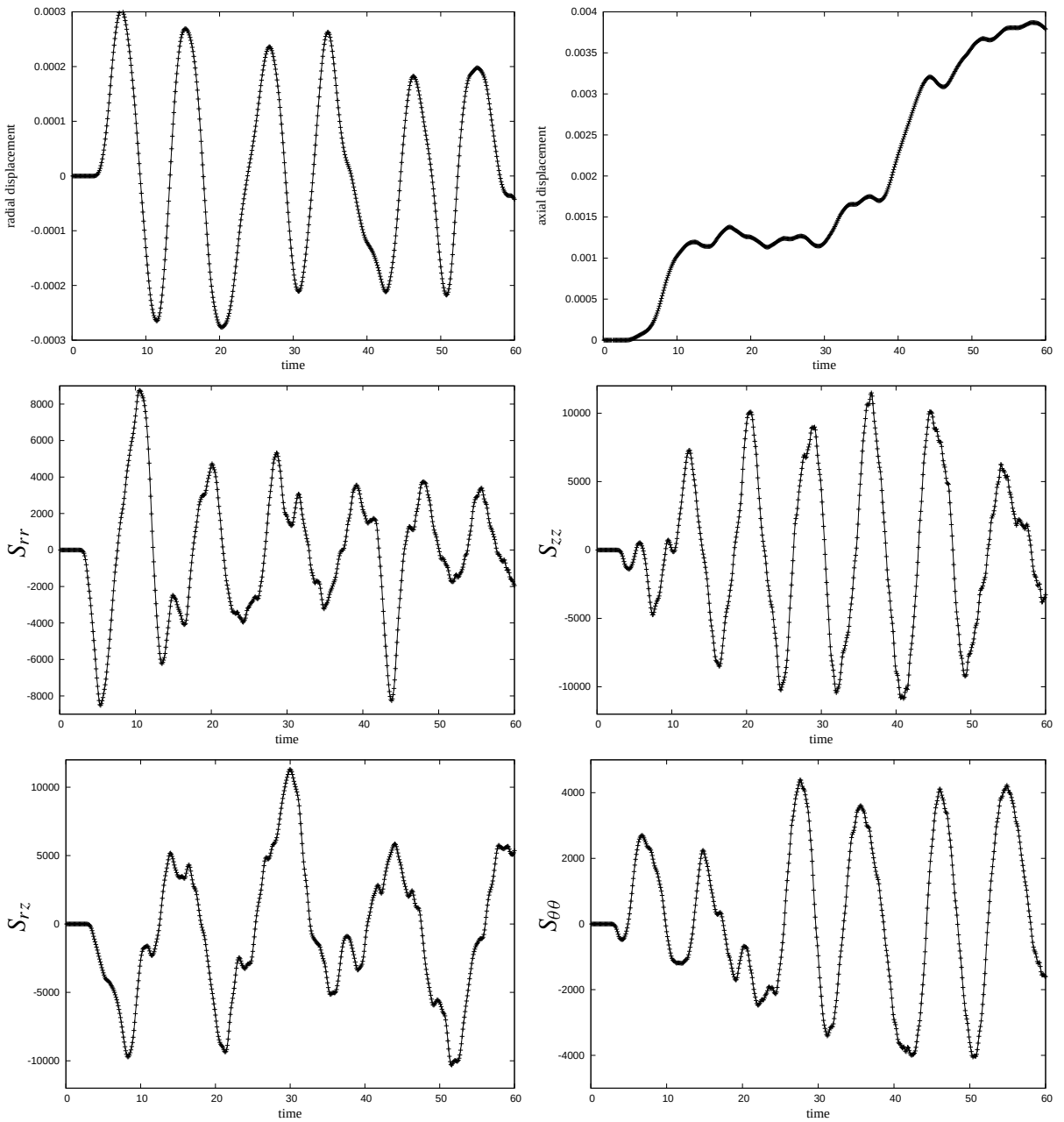

Figure 10. Top row: radial and axial displacement at $(r, z) = (0.7, 0.5)$ as a function of time in the elastic wave propagation problem. Remaining rows: radial, longitudinal, shear and hoop stresses at the same location. Time is measured in μs.

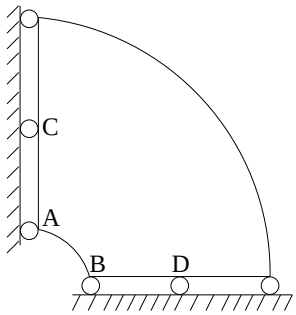

Figure 11. An almost incompressible sphere subjected to internal pressure. Only the part of the domain shown is modelled using axisymmetric elements.

3F. ***Thick almost incompressible sphere subjected to internal pressure.*** This example shows the relative immunity of hybrid elements to volumetric locking under finite deformations when the material is an almost incompressible neo-Hookean material [Heisserer et al. 2008]. The inner radius of the sphere is 10 mm and outer radius is 30 mm. Using symmetry, only a part of the domain is modelled using axisymmetric elements as shown in Figure 11. Meshes of 2×2, 4×4 and 8×8 A9 or B9 elements and 4×4, 8×8 and 16×16 A4 elements are used to discretize the domain. The neo-Hookean material model given by (3-2) with $c_1 = 0.5$ MPa, $\kappa = 10^5$ MPa (which corresponds to a Poisson ratio of 0.499995) is used. The internal pressure is 1 MPa and the outer surface is traction free. The normalized results for the radial displacement at the inner surface, obtained by using the reference solution of 5.50198336 [Heisserer et al. 2008] are presented in Table 3.

While the displacement-based element locks severely, the performance of the hybrid elements, and especially the A9 element even with a very coarse mesh, is quite remarkable. As already mentioned, adding the higher-order terms to $S_{\theta\theta}$ is critical in ensuring the symmetry of the solution at points A and B, although these terms are not required to remove any zero-energy mode. This is yet another example of an improvement of performance by using more (judiciously chosen) terms in the stress interpolation than the minimum number based purely on elimination of zero-energy modes.

Now consider the linear counterpart of this problem. The inner radius and outer radii of the sphere are now 1 and 5, respectively, and the internal pressure is of unit magnitude. The material properties are $E = 1000$ and $\nu = 0.499$. Uniform meshes of 4×4, 8×8 and 16×16 A4, and 2×2, 4×4 and 8×8 A9 meshes are used. The analytical solution for the radial displacement is 7.5556×10^{-4}. The

	Point A			Point B		
Nodes/side	B9	A4	A9	B9	A4	A9
5	0.00040	0.96029	1.01086	0.00040	0.91544	0.99578
9	0.00362	0.99719	1.00278	0.00362	0.97808	1.00094
17	0.05858	1.00076	1.00039	0.05858	0.99447	1.00016

Table 3. Normalized radial displacements at the inner surface in the thick-sphere problem: nonlinear case.

Nodes/side	Point A B9	Point A A4	Point A A9	Point B B9	Point B A4	Point B A9
5	0.03035	0.80279	0.83023	0.03030	0.80482	0.80708
9	0.14847	0.92708	0.95947	0.14846	0.92369	0.95704
17	0.60879	0.97865	0.99528	0.60881	0.97677	0.99504

Table 4. Normalized radial displacement at the inner surface in the thick-sphere problem: linear case.

Nodes per side	Radial stress Point C B9	Point C A4	Point C A9	Point D B9	Point D A4	Point D A9	Hoop stress Point C B9	Point C A4	Point C A9	Point D B9	Point D A4	Point D A9
5	−17.857	0.816	−0.601	−17.857	0.881	−0.465	19.579	0.162	3.122	19.579	1.118	3.061
9	−7.068	0.942	0.750	−7.068	0.930	0.772	8.028	0.800	1.201	8.028	0.990	1.179
17	−5.217	0.980	0.948	−5.217	0.977	0.952	6.965	0.952	1.048	6.965	0.993	1.043

Table 5. Normalized radial and hoop stresses in the thick-sphere problem: linear case.

normalized results obtained are presented in Table 4. Note again the severe locking in the displacement-based elements, and the relative immunity of the hybrid elements.

The results for the radial and hoop stresses (in the spherical coordinate system) at points C and D located at the mean radius as shown in Figure 11, normalized against the analytical values of −0.0292712 and 0.0267324, are presented in Table 5. Note that the even the sign of the radial stress (besides, of course, the magnitude) for the finest B9 mesh is in error.

3G. ***Circular plate subjected to pressure.*** A thin circular plate clamped at its outer edge is subjected to pressure loading as shown in Figure 12. This example has been solved using the p-FEM method in [Yosibash et al. 2007]. The neo-Hookean material model given by (3-2) with $c_1 = 0.5$ MPa and $\kappa = 2000$ MPa (which corresponds to a Poisson ratio of 0.49975) is used. We solve this example using both axisymmetric and wedge/hexahedral elements. This example provides an especially good test for the wedge/hexahedral elements since the mesh is distorted (because of the circular domain that is being modelled), the plate is thin, the material is almost incompressible, and the loading is of follower type so that the stiffness matrix depends on the load. Meshes of 8×1, 16×1 and 32×1 A9 (or B9) elements, 16×2, 32×2 and 64×2 A4 elements, $8 \times 8 \times 1$ ($n_r \times n_\theta \times n_z$), $16 \times 16 \times 1$ and $32 \times 32 \times 1$ W18/S27 (or

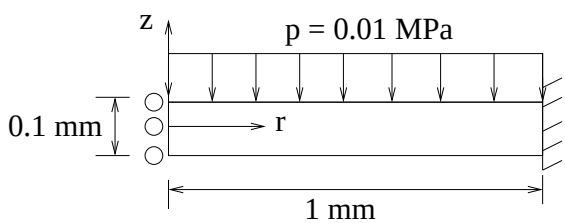

Figure 12. A thin circular plate clamped at its outer edge and subjected to pressure loading.

Nodes/side	Axisymmetric elements			Wedge/hexahedral elements		
	B9	A4	A9	B18/B27	W6/S8	W18/S27
17	0.85562	0.99302	0.98709	0.85559	0.99018	0.98555
33	0.88409	0.99755	0.99524	0.88409	0.99649	0.99456
65	0.89663	0.99996	0.99847	0.89661	0.99956	0.99822

Table 6. Normalized vertical displacement at the center of the top surface of the thin circular plate: nonlinear analysis.

B18/B27) elements, and $16 \times 16 \times 2$, $32 \times 32 \times 2$ and $64 \times 64 \times 2$ W6/S8 elements are used. In the case of wedge/hexahedral elements, only a quarter of the plate is modelled with wedge elements used in the layer closest to the center, and hexahedral elements elsewhere. The displacements at the center of the top surface normalized against the reference solution of 0.182647 [Yosibash et al. 2007] are presented in Table 6.

Note that the results obtained using wedge/hexahedral elements, inspite of the mesh distortion, are almost as good as those obtained using axisymmetric elements. The results for all the hybrid elements are obtained within a total of only 12 iterations. In contrast, the displacement-based elements not only converge very slowly, but also require approximately 280 iterations (spread over 50 load steps) to obtain the solution.

Now consider the linear counterpart of the problem. A simply-supported circular plate of radius 10, and with $\nu = 0.3$, is subjected to a unit pressure load on the top surface. Two cases are considered (i) $E = 10^4$, $h = 1$ ("thick plate"), and (ii) $E = 10^{10}$, $h = 0.01$ ("thin plate"). The analytical solutions for the center-point deflection are 0.70388 and 0.69563, respectively. The normalized results for the center-point deflection are presented in Table 7.

Note the exceptionally high accuracy of the hybrid axisymmetric elements, even when the thickness/radius ratio is as small as 1/1000. One of the interesting features of the stress solution in the thin plate case is that while the A4, A9 and W18/S27 elements yield transverse shear stress values at the

Nodes/side	Thick plate ($h = 1$)					
	B18/B27	W6/S8	W18/S27	B9	A4	A9
5	0.94419	0.88661	0.98465	0.97980	1.02418	1.00277
9	0.99256	0.98659	0.99551	0.99616	1.00749	0.99853
17	0.99551	0.99640	0.99580	0.99607	0.99753	0.99608

Nodes/side	Thin plate (h=0.01)					
	B18/B27	W6/S8	W18/S27	B9	A4	A9
5	0.12700	0.63708	0.44493	0.95746	1.02555	1.00453
9	0.66715	0.87905	0.80732	0.98996	1.00898	0.99954
17	0.93986	0.96304	0.97489	0.99984	1.00020	0.99989

Table 7. Normalized center-point displacements in the simply-supported circular plate problem: linear analysis.

center of the plate that are close to zero, the B9 element yields values ranging from 175 to 2600, while the other elements in the table, and the W21 of [Jog 2005] yield values of the order of 10^5!

3H. ***Large strain vibration of a long half cylinder.*** The base of a half-cylinder travelling with a uniform initial velocity v is suddenly brought to rest as shown in Figure 13, left, due to which it vibrates from left to right. This example was solved in [Bonet et al. 2001] using an averaged nodal deformation gradient formulation. The neo-Hookean material model given by (3-2) is used, with $c_1 = 1.7855 \times 10^5$ Pa and $\kappa = 1.667 \times 10^6$ Pa, and the density is 1000 kg/m^3. Uniform meshes $n_r \times n_\theta \times n_z$ of $4 \times 8 \times 40$ W18/S27 (or B18/B27) and $8 \times 16 \times 80$ W6/S8 elements, and a time step $t_\Delta = 0.0025$ s is used. The deformed centerline at various times is shown in Figure 14, left, and should be compared with Figure 4 of [Bonet et al. 2001].

Although the solutions are shown for the W18/S27 mesh, almost identical solutions are obtained with the W6/S8 and B18/B27 meshes. Moreover, almost identical solutions are also obtained with coarser meshes of $2 \times 4 \times 20$ W18/S27 (or B18/B27) and $4 \times 8 \times 40$ W6/S8 elements, and a time step $t_\Delta = 0.005$ s, showing convergence with respect to mesh refinement. Since the velocity is zero at the base, and since the remaining surface is traction free, the total energy (kinetic+strain energy) should be conserved by the numerical algorithm. As is seen from Figure 14, right, this is achieved by our numerical algorithm. We would like to state that the use of an interpolation obtained by *excluding* Rule (2) fails to converge (after a few time steps) on this problem showing the importance of this rule.

3I. ***Inflation of a square airbag.*** This example, in which a flat square isotropic membrane is gradually inflated by a constant pressure until its magnitude reaches 5 kPa, has been solved using a wrinkling model in [Jarasjarungkiat et al. 2009]. The geometry and material properties are shown in Figure 13, right.

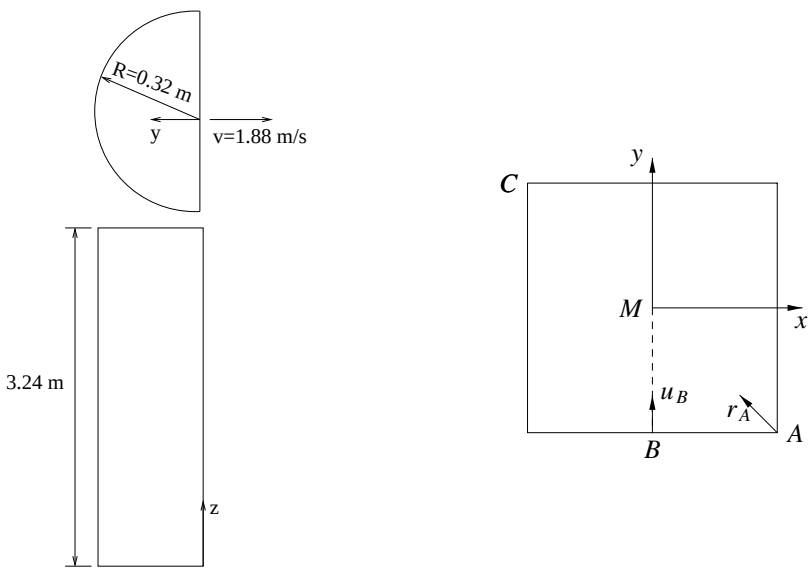

Figure 13. Left: geometry and initial conditions for the long half cylinder problem. Right: geometry and material properties for the airbag problem. The thickness is 0.06 cm, the length AC is 120 cm, and $E = 58.8$ kN/cm^2, $v = 0.4$.

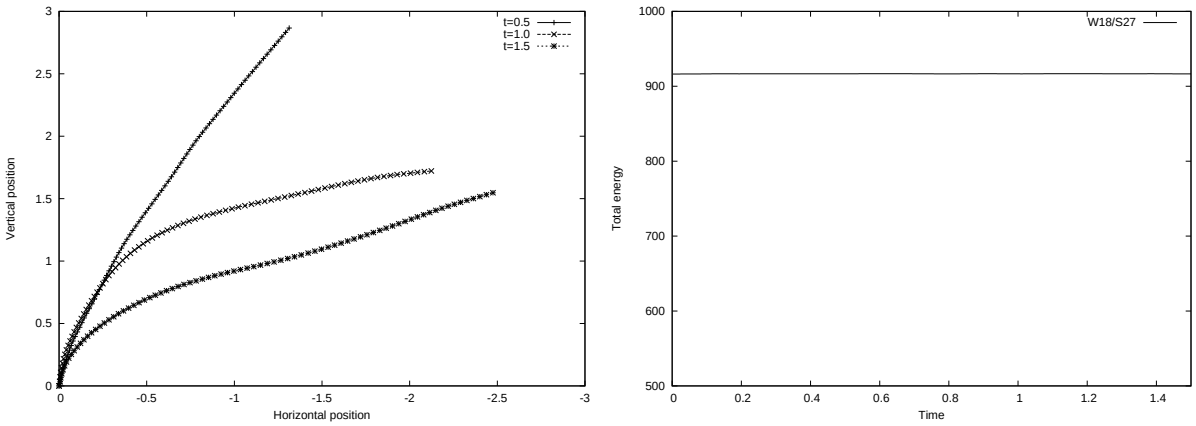

Figure 14. Long half cylinder problem, W18/S27 mesh: deformed centerline of the semicircle at various times (left) and total energy as a function of time (right).

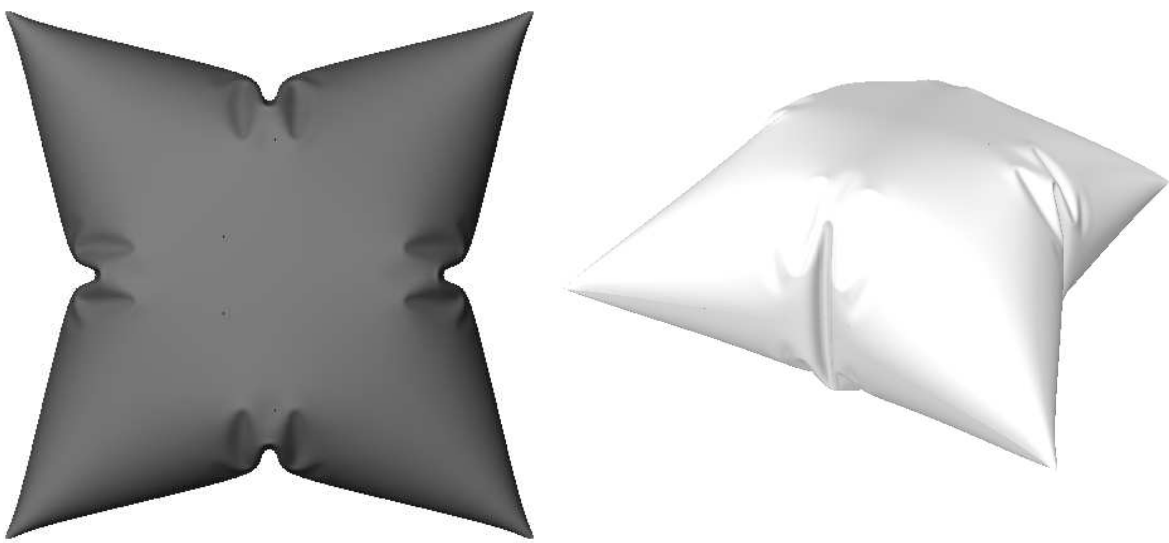

Figure 15. Top and isometric views of the inflated airbag.

Due to the presence of wrinkles, the stiffness matrix can become singular, and hence we solve this problem using the transient algorithm described in [Jog and Motamarri 2009] with an appropriate amount of damping to damp out the transients, and reach to a steady-state solution. A $50 \times 50 \times 1$ mesh of 27-node hybrid hexahedral elements is used to discretize a quarter of the domain due to symmetry. The total pressure of 5 kPa is applied gradually in a linearly varying fashion over the time interval [0, 5], and then maintained constant after that. The time step used in the transient analysis is $t_\Delta = 0.002$. The values of density ρ and damping parameter α used are 2700 kg/m^3 and 10^6, respectively. The steady-state solution is reached after 6 seconds, and is shown in Figure 15.

In contrast to solutions obtained using wrinkle models, the strategy above yields the details of the wrinkles (including the wavelength and amplitude), and accurate values of stresses within the entire

membrane. The values of the displacement w_M, r_A and u_B (in cm) obtained using our method are (21.45, 4.63, 16.63), while the values presented in [Jarasjarungkiat et al. 2009] are (21.669, 6.92, 12.37). The reason for the significant difference in the displacement at point B is that, in reality, there is a sharp ridge around that point (see Figure 15), which is smoothened out when one uses a wrinkle model, as in Figure 6 of that reference.

4. Conclusions

The use of a minimal stress interpolation that does not satisfy the rules enumerated in this work, often results in instabilities, non-convergence or spurious stresses. As shown by means of several examples, stress interpolations obeying these rules result in increased robustness. Although the number of interpolation terms in some of the higher-order elements, such as the 27-node hexahedral and the 9-node axisymmetric elements, is much more than the minimum required, their performance continues to be far superior to the displacement-based elements, and in many problems superior to the 8-node hexahedral and 4-node axisymmetric hybrid elements, respectively. More importantly, they result in far greater robustness, especially in transient simulations, where, as our numerical experiments show, stable solutions are obtained even over very long time simulations. Another advantage is that the rules enumerated, since they require the polynomials to be complete in some sense, result in a unique interpolation function for the stresses. One of the interesting conclusions in the case of the 8-node and 27-node hexahedral elements, the 18-node wedge element, and the 4-node and 9-node axisymmetric elements is that for a robust formulation, the normal stress interpolations (except, of course, the hoop stress interpolation in the case of axisymmetric elements) are obtained simply by differentiating the displacement field, while the interpolations for the shear stress components S^{ij} are composed of terms that are common to the interpolations for the normal stresses S^{ii} and S^{jj}.

References

[Bonet et al. 2001] J. Bonet, H. Marriott, and O. Hassan, "An averaged nodal deformation gradient linear tetrahedral element for large strain explicit dynamic applications", *Comput. Methods Appl. Mech. Engrg.* **17** (2001), 551–561.

[Cherukuri and Shawki 1996] H. P. Cherukuri and T. G. Shawki, "A finite-difference scheme for elastic wave propagation in a circular disk", *J. Acoust. Soc. Amer.* **100**:4 (1996), 2139–2155.

[Danielson and Tielking 1993] K. T. Danielson and J. T. Tielking, "Fourier continuum finite elements for large deformation problems", *Comput. and Structures* **49** (1993), 133–147.

[Gupta 2000] A. Gupta, "WSMP: Watson Sparse Matrix Package, II: direct solution of general sparse systems", Research Report RC 21888 (98472), IBM, 2000.

[Gupta 2002] A. Gupta, "Recent advances in direct methods for solving unsymmetric sparse systems of linear equations", *ACM Trans. Math. Software* **28**:3 (2002), 301–324.

[Heisserer et al. 2008] U. Heisserer, S. Hartmann, A. Düster, and Z. Yosibash, "On volumetric locking-free behaviour of p-version finite elements under finite deformations", *Comm. Numer. Methods Engrg.* **24**:11 (2008), 1019–1032.

[Jarasjarungkiat et al. 2009] A. Jarasjarungkiat, R. Wuchner, and K. U. Bletzinger, "Efficient sub-grid scale modeling of membrane wrinkling by a projection method", *Comput. Methods Appl. Mech. Engrg.* **198** (2009), 1097–1116.

[Jog 2005] C. S. Jog, "A 27-node hybrid brick and a 21-node hybrid wedge element for structural analysis", *Finite Elem. Anal. Des.* **41** (2005), 1209–1232.

[Jog and Annabatula 2006] C. S. Jog and R. Annabatula, "The development of hybrid axisymmetric elements based on the Hellinger–Reissner variational principle", *Internat. J. Numer. Methods Engrg.* **65** (2006), 2279–2291.

[Jog and Kelkar 2006] C. S. Jog and P. P. Kelkar, "Non-linear analysis of structures using high performance hybrid elements", *Internat. J. Numer. Methods Engrg.* **68**:4 (2006), 473–501.

[Jog and Motamarri 2009] C. S. Jog and P. Motamarri, "An energy-momentum conserving algorithm for nonlinear transient analysis within the framework of hybrid elements", *J. Mech. Mater. Structures* **4**:1 (2009), 157–186.

[Lee and Rhiu 1986] S. W. Lee and J. J. Rhiu, "A new efficient approach to the formulation of mixed finite element models for structural analysis", *Internat. J. Numer. Methods Engrg.* **23** (1986), 1629–1641.

[Lo and Ling 2000] S. H. Lo and C. Ling, "Improvement on the 10-node tetrahedral element for three-dimensional problems", *Comput. Methods Appl. Mech. Engrg.* **189** (2000), 961–974.

[Pian and Sumihara 1984] T. H. H. Pian and K. Sumihara, "Rational approach for assumed stress finite elements", *Internat. J. Numer. Methods Engrg.* **20** (1984), 1685–1695.

[Pian and Tong 1986] T. H. H. Pian and P. Tong, "Relations between incompatible displacement model and hybrid stress model", *Internat. J. Numer. Methods Engrg.* **22**:1 (1986), 173–181.

[Punch and Atluri 1984] E. F. Punch and S. N. Atluri, "Development and testing of stable, invariant, isoparametric curvilinear 2- and 3-d hybrid-stress elements", *Comput. Methods Appl. Mech. Engrg.* **47** (1984), 331–356.

[Reese et al. 2000] S. Reese, P. Wriggers, and B. D. Reddy, "A new locking-free brick element technique for large deformation problems in elasticity", *Comput. and Structures* **75**:3 (2000), 291–304.

[Rhiu and Lee 1987] J. J. Rhiu and S. W. Lee, "A new efficient mixed formulation for thin shell finite element models", *Internat. J. Numer. Methods Engrg.* **24** (1987), 581–604.

[Simo et al. 1989] J. C. Simo, D. D. Fox, and M. S. Rifai, "On a stress resultant geometrically exact shell model, II: the linear theory; computational aspects", *Comput. Methods Appl. Mech. Engrg.* **73**:1 (1989), 53–92.

[Sze et al. 2004a] K. Y. Sze, X. H. Liu, and S. H. Lo, "Hybrid-stress six-node prismatic elements", *Internat. J. Numer. Methods Engrg.* **61** (2004), 1451–1470.

[Sze et al. 2004b] K. Y. Sze, X. H. Liu, and S. H. Lo, "Popular benchmark problems for geometric nonlinear analysis of shells", *Finite Elem. Anal. Des.* **40** (2004), 1551–1569.

[Xue et al. 1985] W.-M. Xue, L. A. Karlovitz, and S. N. Atluri, "On the existence and stability conditions for mixed-hybrid finite element solutions based on Reissner's variational principle", *Internat. J. Solids Structures* **21**:1 (1985), 97–116.

[Yosibash et al. 2007] Z. Yosibash, S. Hartmann, U. Heisserer, and A. Duster, "Axisymmetric pressure boundary loading for finite deformation analysis using p-FEM", *Comput. Methods Appl. Mech. Engrg.* **196** (2007), 1261–1277.

Received 17 Feb 2010. Revised 28 Jun 2010. Accepted 1 Jul 2010.

C. S. JOG: jogc@mecheng.iisc.ernet.in
Department of Mechanical Engineering, Indian Institute of Science, Bangalore 560012, India

JOURNAL OF MECHANICS OF MATERIALS AND STRUCTURES

http://www.jomms.org

Founded by Charles R. Steele and Marie-Louise Steele

See inside back cover or http://www.jomms.org for submission guidelines.

JoMMS (ISSN 1559-3959) is published in 10 issues a year. The subscription price for 2010 is US $500/year for the electronic version, and $660/year (+$60 shipping outside the US) for print and electronic. Subscriptions, requests for back issues, and changes of address should be sent to Mathematical Sciences Publishers, Department of Mathematics, University of California, Berkeley, CA 94720–3840.

JoMMS peer-review and production is managed by EditFLOW™ from Mathematical Sciences Publishers.

PUBLISHED BY

mathematical sciences publishers

http://www.mathscipub.org

A NON-PROFIT CORPORATION

Typeset in LaTeX

Journal of Mechanics of Materials and Structures

Volume 5, No. 3 March 2010